

Monodromy of the quantum 1:1:2 resonant swing spring

A. Giacobbe^{a)} and R. H. Cushman^{b)}

Mathematics Institute, University of Utrecht, 3508 TA Utrecht, The Netherlands

D. A. Sadovskii^{c)} and B. I. Zhilinskiĭ^{d)}

Université du Littoral, UMR du CNRS 8101, 59140 Dunkerque, France

(Received 24 March 2004; accepted 24 August 2004; published 2 December 2004)

We describe the qualitative features of the joint spectrum of the quantum 1:1:2 resonant swing spring. The monodromy of the classical analogue of this problem is studied in Dullin *et al.* [*Physica D* **190**, 15–37 (2004)]. Using symmetry arguments and numerical calculations we compute its three-dimensional (3D) lattice of quantum states and show that it possesses a codimension 2 defect characterized by a nontrivial 3D-monodromy matrix. The form of the monodromy matrix is obtained from the lattice of quantum states and depends on the choice of an elementary cell of the lattice. We compute the quantum monodromy matrix, that is the inverse transpose of the classical monodromy matrix. Finally we show that the lattice of quantum states for the 1:1:2 quantum swing spring can be obtained—preserving the symmetries—from the regular 3D-cubic lattice by means of three “elementary monodromy cuts.” © 2004 American Institute of Physics.

[DOI: 10.1063/1.1811788]

I. INTRODUCTION

The swing spring is a simple mechanical system consisting of a spring of length ℓ and spring constant k with one end attached at a fixed point (the origin of a Cartesian system) and with a weight of mass m attached at the other end. This system admits a Hamiltonian formulation in which the phase space is \mathbb{R}^6 with coordinates x, y, z, p_x, p_y, p_z and symplectic form $dx \wedge dp_x + dy \wedge dp_y + dz \wedge dp_z$. The Hamiltonian function H is

$$(x, y, z, p_x, p_y, p_z) \mapsto \frac{1}{2m}(p_x^2 + p_y^2 + p_z^2) + mgz + \frac{k}{2}(\ell - \sqrt{x^2 + y^2 + z^2})^2. \quad (1)$$

Note that ℓ is the same as ℓ_0 in Refs. 11 and 17.

When the physical parameters are chosen so that $3gm = k\ell$, which is equivalent to requiring that the frequencies of small oscillations of the swing spring near the stable equilibrium are in a 1:1:2 resonance (the only resonance with cubic secular terms), the swing spring has some remarkable features: energy exchange and precession of the swing plane.^{11,17} These characteristics have been widely studied (see Ref. 17 for a comprehensive bibliography), but the information hidden in this classical mechanical system has not been exhausted by these investigations. In fact, the resonant swing spring is a model for molecules such as CO_2 (a textbook example of a 1:1:2 Fermi resonance between stretching and doubly degenerate bending vibration states^{4,13}), HCP ,¹⁸ and a whole class of CHX_3 molecules which possess a Fermi resonance between the CH stretching and bending vibrational states.¹⁹

^{a)}Electronic mail: giacobbe@math.unipd.it

^{b)}Electronic mail: cushman@math.uu.nl

^{c)}Electronic mail: sadovski@univ-littoral.fr

^{d)}Electronic mail: zhilin@univ-littoral.fr

We define the integrable approximation of the swing spring system and discuss the range of energies in which our approximating Hamiltonian gives data that can be considered reliable for the original system. After explaining the origin of the continuous and discrete symmetries of our approximation, we define the quantum analogue of the system and proceed to analyze its quantum spectrum. As the classical swing spring is a three degree of freedom system, its spectrum is represented by a three-dimensional (3D) lattice of points in the space of the values of quantized actions and energy. The main purpose of this work is to show how the nontrivial monodromy of the classical system^{2,3,5} manifests itself (1) as a defect of this lattice and (2) in the distribution of quantum states with respect to quantum numbers which can be predicted from the theorem of Duistermaat–Heckman.¹⁰

Fixing a global quantum number associated to the momentum corresponding to a circle symmetry, we first analyze the quantum lattice of two-dimensional (2D) slices of the swing spring quantum spectrum and find that the monodromy computed in such slices gives insufficient information to determine the monodromy of the full 3D quantum spectrum. We proceed with the investigation of the 3D quantum lattice by giving two methods to compute the quantum monodromy matrix. The first method, presented in Ref. 26, requires the introduction of quantum defects in the regular \mathbb{Z}^3 lattice. In order to preserve the discrete symmetries of the system, one must use three elementary defects to obtain the quantum lattice. The second method obtains the quantum monodromy matrix directly by moving an elementary cell in the three-dimensional quantum lattice.

II. CLASSICAL AND QUANTUM 1:1:2 SWING SPRING

The swing spring is a Hamiltonian system on $(\mathbb{R}^6, dx \wedge dp_x + dy \wedge dp_y + dz \wedge dp_z)$ with Hamiltonian H given by (1). Despite it being a chaotic dynamical system,¹⁶ the motions of the swing spring near the stable equilibrium located at $p_0 = (0, 0, -\ell - mg/k, 0, 0, 0)$ have a clear quasiperiodic behavior when the parameters are chosen so that the characteristic oscillations of the system are tuned in 1:1:2 resonance.

To study this behavior we will begin by considering the Taylor expansion of H around p_0 . The quadratic part of the Taylor expansion of H at p_0 is

$$H_2 = \frac{1}{2m}(p_x^2 + p_y^2 + p_z^2) + \frac{k}{2} \left(\frac{gm}{k\ell + gm} x^2 + \frac{gm}{k\ell + gm} y^2 + z^2 \right).$$

To have a 1:1:2 harmonic oscillator as dominant term, the physical coefficients in H_2 must satisfy the condition $3gm = k\ell$. Assuming this and making the change of coordinates

$$x \mapsto \sqrt[4]{\frac{4}{km}} \xi, \quad y \mapsto \sqrt[4]{\frac{4}{km}} \eta, \quad z \mapsto \sqrt[4]{\frac{1}{km}} \zeta, \quad p_x \mapsto \sqrt[4]{\frac{km}{4}} p_\xi, \quad p_y \mapsto \sqrt[4]{\frac{km}{4}} p_\eta, \quad p_z \mapsto \sqrt[4]{km} p_\zeta,$$

we find that

$$H_2 = \frac{1}{2} \hbar (\xi^2 + p_\xi^2 + \eta^2 + p_\eta^2 + 2\zeta^2 + 2p_\zeta^2)$$

and the Taylor expansion of H (1) about p_0 up to sixth order terms becomes

$$H_{\text{trunc}} = H_2 - \frac{3}{8} \hbar^{3/2} \zeta (\eta^2 + \xi^2) + \frac{3}{64} \hbar^2 (\eta^2 + \xi^2) (-2\zeta^2 + \eta^2 + \xi^2) - \frac{3}{256} \hbar^{5/2} \zeta (\eta^2 + \xi^2) (2\zeta^2 - 3(\eta^2 + \xi^2)) - \frac{3}{1024} \hbar^3 (\eta^2 + \xi^2) (2\zeta^4 - 6\zeta^2(\eta^2 + \xi^2) + (\eta^2 + \xi^2)^2), \tag{2}$$

where $\hbar = \sqrt{k^3/(g^4 m^5)}$. To obtain (2) we have rescaled H_{trunc} to remove the factor $g^2 m^2/(2k)$ and dropped an additive constant. The original Hamiltonian H (1), and thus the Hamiltonian H_{trunc} (2), has an $\text{SO}(2)$ axial symmetry

$$(\xi, \eta, \zeta, p_\xi, p_\eta, p_\zeta) \mapsto \left(R_t \begin{pmatrix} \xi \\ \eta \\ \zeta \end{pmatrix}, R_t \begin{pmatrix} p_\xi \\ p_\eta \\ p_\zeta \end{pmatrix} \right).$$

Here

$$R_t = \begin{pmatrix} \cos t & -\sin t & 0 \\ \sin t & \cos t & 0 \\ 0 & 0 & 1 \end{pmatrix}$$

is a rotation about the ζ axis lifted to the full phase space \mathbb{R}^6 . The momentum of this symmetry is the function $L = \xi p_\eta - \eta p_\xi$.

It is convenient to perform another coordinate change, namely

$$\xi \mapsto \frac{1}{\sqrt{2}}(p_2 + q_1), \quad \eta \mapsto \frac{1}{\sqrt{2}}(p_1 + q_2), \quad \zeta \mapsto q_3, \quad p_\xi \mapsto \frac{1}{\sqrt{2}}(p_1 - q_2), \quad p_\eta \mapsto \frac{1}{\sqrt{2}}(p_2 - q_1), \quad p_\zeta \mapsto p_3.$$

This brings the momentum L into diagonal form $\frac{1}{2}(q_2^2 + p_2^2 - q_1^2 - p_1^2)$ and does not change the quadratic part H_2 of the Hamiltonian H_{trunc} .

Bringing H_{trunc} into normal form with respect to H_2 up to order 6, one obtains the Hamiltonian $H_{\text{nf}}^{(6)}$. This is the polynomial Hamiltonian (as well as its truncation $H_{\text{nf}}^{(3)}$ to third order) whose quantum spectrum we analyze in Secs. III–V.

A. Lie symmetry of classical and quantum system

The sixth order normalized Hamiltonian $H_{\text{nf}}^{(6)}$ defines a three degree of freedom system with two integrals of motion: L , the momentum associated to the axial symmetry and N , the quadratic part H_2 of the normalized Hamiltonian, which is the same as the quadratic part of the original Hamiltonian H . The flows of the Hamiltonian vector fields associated to these integrals commute and define a 2-torus action that preserves $H_{\text{nf}}^{(6)}$. Thus L and N together with the Hamiltonian $H_{\text{nf}}^{(6)}$ form a completely integrable system.

Being $S^1 \times \text{SO}(2)$ -invariant, the normalized Hamiltonian $H_{\text{nf}}^{(6)}$ can be written as a polynomial in the generators of the ring of $S^1 \times \text{SO}(2)$ -invariant functions. The Molien generating function²⁰ (A7) indicates that this ring is generated by five invariants, three quadratic and two cubic, see Appendix A 1. These invariants can be chosen to be

$$N = \frac{1}{2}(q_1^2 + p_1^2 + q_2^2 + p_2^2 + 2q_3^2 + 2p_3^2), \quad (3a)$$

$$R = \frac{1}{2}(q_1^2 + p_1^2 + q_2^2 + p_2^2), \quad (3b)$$

$$L = \frac{1}{2}(-q_1^2 - p_1^2 + q_2^2 + p_2^2), \quad (3c)$$

$$S = (q_1 p_2 + q_2 p_1) q_3 - (q_1 q_2 - p_1 p_2) p_3, \quad (3d)$$

$$T = (q_1 q_2 - p_1 p_2) q_3 + (q_1 p_2 + q_2 p_1) p_3, \quad (3e)$$

and they are subject to the relations (A9).

B. Normalized system and its analysis

The normalized Hamiltonian $H_{\text{trunc}}(2)$ written in terms of the invariants (3) is

$$\begin{aligned}
 H_{\text{nf}}^{(6)} = & \hbar N - \frac{3}{16} \hbar^{3/2} S - \frac{57}{1024} \hbar^2 NR + \frac{177}{2048} \hbar^2 R^2 - \frac{39}{2048} \hbar^2 L^2 - \frac{819}{65\,536} \hbar^{5/2} NS + \frac{2151}{65\,536} \hbar^{5/2} RS - \frac{8025}{4\,194\,304} \hbar^3 N^2 R \\
 & + \frac{7623}{2\,097\,152} \hbar^3 NR^2 + \frac{6879}{2\,097\,152} \hbar^3 R^3 - \frac{6555}{2\,097\,152} \hbar^3 NL^2 + \frac{4803}{4\,194\,304} \hbar^3 RL^2 - \frac{1089}{262\,144} \hbar^3 S^2. \tag{4}
 \end{aligned}$$

Note that powers of T higher than 1 should not appear in (4) since the invariants satisfy the relation (A9). Furthermore, (4) does not include any power of N higher than 1 because the swing spring (1) contains a two degree of freedom harmonic oscillator as subsystem. Other special features of $H_{\text{nf}}^{(6)}$ are related to the discrete symmetries described below.

In most of what follows, we describe the quantum spectrum of the Hamiltonian S instead of that of $H_{\text{nf}}^{(6)}$. Of course, (S, L, N) is also a completely integrable system. At first order the difference between the Hamiltonian S and (4) is given by $H \mapsto -(16/3\hbar^{3/2})(H - \hbar N)$. This means that to first order for any given value of N the quantum spectra of H and S coincide up to a translation and dilation.

The energy-momentum map

$$\mathcal{EM}: \mathbb{R}^6 \rightarrow \mathbb{R}^3 \quad (q, p) \mapsto (S(q, p), L(q, p), N(q, p))$$

is widely used in our analysis. Its image $U \subset \mathbb{R}^3$ and the corresponding bifurcation diagram is described in Ref. 11 and Appendix A 3. $U_{\text{reg}} \subset U$ is the set of regular values which represent regular tori \mathbb{T}^3 . Points of the boundary ∂U represent equilibria relative to the $\mathbb{T}^2 = S^1 \times \text{SO}(2)$ action. The main feature to note is that $U \setminus U_{\text{reg}}$ also contains a thread of singular values inside U , which represent a special singular 3D fiber described in Appendix A 3.

It can be shown that the system $(H_{\text{nf}}^{(6)}, L, N)$ is qualitatively the same as (S, L, N) for sufficiently small values of N . In particular it has qualitatively the same energy-momentum map and corresponding 3D quantum lattice. The concrete estimate of the upper limit for N can be obtained from the analysis of the slope of $S(R)$ at $R=L=0$ of $H_{\text{nf}} = \text{const}$. Specifically, $|dS/dR|$ should be smaller than the slope at the conical singular point of the reduced space, see Appendix A 2. In particular considering the terms of order \hbar^2 we obtain $N < 2^{12} 19^{-2} \hbar^{-1}$.

C. Discrete symmetries and a pseudosymmetry

The normalized Hamiltonian $H_{\text{nf}}^{(6)}$ (4) is not a generic $S^1 \times \text{SO}(2)$ -symmetric polynomial in the invariants, because (4) does not contain terms of odd degree in L or any power of T . The reason for this is that the original Hamiltonian (1) has a $\mathbb{Z}_2 \times \mathbb{Z}_2$ discrete symmetry group generated by

$$\mathcal{T}: (x, y, z, p_x, p_y, p_z) \mapsto (x, y, z, -p_x, -p_y, -p_z),$$

$$\mathcal{T}_s: (x, y, z, p_x, p_y, p_z) \mapsto (y, x, z, -p_y, -p_x, -p_z),$$

$$\sigma_v: (x, y, z, p_x, p_y, p_z) \mapsto (y, x, z, p_y, p_x, p_z).$$

Note that $\mathcal{T}_s = \mathcal{T} \circ \sigma_v = \sigma_v \circ \mathcal{T}$ and that the square of each generator is the identity. This discrete symmetry survives truncation and normalization. It induces the following transformations on the invariants:

$$\mathcal{T}: (N, R, L, S, T) \mapsto (N, R, -L, S, -T), \tag{5a}$$

$$\mathcal{T}_s: (N, R, L, S, T) \mapsto (N, R, L, S, -T), \tag{5b}$$

$$\sigma_v: (N, R, L, S, T) \mapsto (N, R, -L, S, T). \tag{5c}$$

From (5) we see that the functions T and L are not invariant of the $\mathbb{Z}_2 \times \mathbb{Z}_2$ action. This explains the absence of odd powers of L and T in (4).

To analyze the model system (S, L, N) we also consider the involution

$$(\xi, \eta, \zeta, p_\xi, p_\eta, p_\zeta) \mapsto (-\xi, -\eta, -\zeta, -p_\xi, -p_\eta, -p_\zeta), \quad (6a)$$

which acts on the invariants as

$$(N, R, L, S, T) \mapsto (N, R, L, -S, -T). \quad (6b)$$

As the transformation (6a) maps S to $-S$, we call it a pseudosymmetry. We will exploit this pseudosymmetry below. In particular the image of the energy-momentum map of (S, L, N) is symmetric with respect to (6b). Similarly, the corresponding 3D quantum lattice is symmetric with respect to the plane $S=0$.

D. Classical integrals, quantum numbers, and joint quantum spectrum

Each of the functions in the integrable system (S, L, N) can be quantized according to the rules discussed in Appendix B. The corresponding three quantum operators \hat{N} , \hat{L} , and \hat{S} are self-adjoint and commute. Hence they can be simultaneously diagonalized. In Appendix B we give the details of the calculation of the joint quantum spectrum of $(\hat{S}, \hat{L}, \hat{N})$ and of the quantum analogue of $H_{\text{nf}}^{(6)}$. We also explain the decomposition of the domain of the quantum operators that allows us to numerically compute the quantum spectrum. To every common eigenspace one can associate a triple of real numbers and plot these triples in \mathbb{R}^3 , generating a lattice of quantum states represented as points in 3-space. This 3D lattice of points fits in the image of the classical energy-momentum map \mathcal{EM} of the integrable system (S, L, N) , a description of which is in Appendix A 3. Similarly the quantum lattice for the swing spring $(H_{\text{nf}}^{(6)}, L, N)$ fits inside the respective \mathcal{EM} image.

Definition 1: The lattice of quantum states of $(\hat{H}, \hat{L}, \hat{N})$ superimposed to the image of the \mathcal{EM} map of the corresponding classical completely integrable system (H, L, N) is called the *quantum diagram*. A *polyad quantum number* is an injective integer labeling of the eigenvalues of the quantum operator \hat{N} . A *local quantum number* is an injective integer labeling of the eigenspaces of a quantum operator associated to a local action variable for the completely integrable quantum system $(\hat{H}, \hat{L}, \hat{N})$. A *local action variable* is a function locally defined on phase space whose Hamiltonian vector field has a 2π -periodic flow and Poisson commutes with the classical Hamiltonian H and the momenta N and L .

The notion of polyad quantum number is well established in the theoretical chemistry and molecular physics community.²⁴ Both polyad and local quantum numbers label eigenspaces with large dimension, that is, eigenvalues with high multiplicity. A choice of labeling of the points of the quantum spectrum corresponding to the quantum numbers of a global action will be referred to as *global quantum number*. The definition of global quantum numbers, as opposed to the choice of a quantum number, which is just a labeling of eigenspaces of a quantum spectrum, is at the heart of the presentation to follow.

Since the systems with Hamiltonian $H=S$ and $H=H_{\text{nf}}^{(6)}$ are qualitatively the same, we will use $H=S$ which is easier to study analytically.

Lemma 1: The eigenstates of the quantum system $(\hat{S}, \hat{L}, \hat{N})$ can be labeled by three quantum numbers related to the three commuting operators \hat{S} , \hat{N} , and \hat{L} :

- (i) The global quantum number $n_N=0, 1, 2, \dots$ can be chosen to be the eigenvalue of the operator \hat{N} and is the total number of quanta for the 1:1:2 resonance oscillator or the *polyad* quantum number. The total number of quantum states within one n_N -polyad equals

$$\mathcal{N}(n_N) = \begin{cases} \left(\frac{1}{2}n_N + 1\right)^2 & \text{if } n_N \text{ is even,} \\ \left(\frac{1}{2}n_N + 1\right)^2 - \frac{1}{4} & \text{if } n_N \text{ is odd.} \end{cases}$$

- (ii) The global quantum number n_L can be chosen to be the eigenvalue of the operator \hat{L} and is the projection of the angular momentum on the axis of symmetry. For each n_N , the quantum number n_L takes (n_N+1) different values

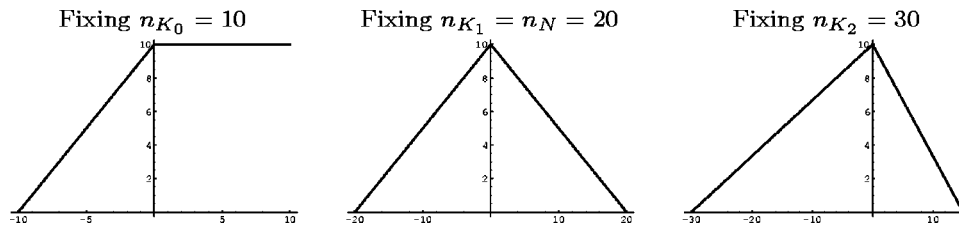


FIG. 1. The plot of the number of states in the slice having a fixed n_{K_m} quantum number as a function of the quantum number n_L .

$$n_L = n_N, n_N - 2, \dots, -n_N + 2, -n_N.$$

The total number of states for each fixed value of n_N and n_L equals

$$\mathcal{N}(n_N, n_L) = \frac{1}{2}(n_N - |n_L|) + 1.$$

- (iii) A quantum number n_S labels the eigenspaces within the set of states with the same n_L and n_N according to the energy of the system.

Instead of using the natural momenta N and L , one could use the momentum

$$K_m = (m + 1)N + (m - 1)L \tag{7}$$

together with L . The number of states in a fixed quantum level of the operator \hat{K}_m can be thought as a function of n_L . A computation shows that this function assigns to every n_L in $[-n_{K_m}, 0]$ the natural number $(n_L + n_{K_m}) / (m + 1)$ and to every n_L in $[0, n_{K_m} / m]$ the natural number $(-n_L m + n_{K_m}) / (m + 1)$. The cases corresponding to $m = 0, 1, 2$ are plotted in Fig. 1.

A classical formula states that the number of quantum states of a given quantum system is \hbar -proportional to the symplectic area of the phase space in which the system is defined. Hence, the graphs in Fig. 1 can also be obtained by first reducing \mathbb{R}^6 with respect to the circle action with momentum K_m , which defines the manifold M_k , and then by plotting the L -dependent symplectic volume of the manifold M_k reduced with respect to the circle action with momentum L . These volumes can be computed directly from the theorem of Duistermaat and Heckman, see Refs. 10 and 15. In Ref. 14 this theorem was applied to the analysis of a three-dimensional quantum problem with monodromy.

The theorem of Duistermaat and Heckman states that the cohomology class of the symplectic form of a symplectically T^n -reduced space varies piecewise linearly with the values of the momentum map. To be more precise denote by M_x the symplectic manifold obtained by symplectically reducing a manifold M with respect to the T^n -action above the value x in \mathfrak{t}^* . Let a be a regular value of the momentum map, let b be an element in \mathfrak{t}^* , and let t be a small real number. The manifold M_{a+tb} is diffeomorphic to M_a . Both manifolds are base spaces of diffeomorphic principal T^n bundles. The symplectic forms of M_a and M_{a+tb} define cohomology classes that differ by the class $t\langle b, c \rangle$, where c is the Chern class of the torus bundle over M_a , that is, an element of $H^2(M_a) \otimes \mathfrak{t}$, and $\langle \cdot, \cdot \rangle$ is the pairing between the Lie algebra \mathfrak{t} and its dual \mathfrak{t}^* . Observe that $t\langle b, c \rangle$ is a function linear in t . Crossing the set of critical values of the T^n -momentum map, the Chern class, and hence the slope of the linear function changes into $\langle b, c' \rangle$. Since the volume form of a symplectic manifold is an appropriate power of the symplectic form, it changes polynomially in t .

In our case we are given a T^2 action having the tuple (N, L) for momentum map. The momentum polytope is the convex solid wedge with boundaries $0 \leq N = L$ and $0 \leq N = -L$. In addition to this boundary, the set of critical values of the T^2 -momentum map also contains the line $L = 0$. The fiber of the T^2 -momentum map over values in the set $E^+ = \{L > 0, L < N\}$ is a 2-torus bundle over a 2-sphere with Chern class $(\omega_{\xi_N} + \omega_{\xi_L}) / 2$; while that above values in the set

$E^- = \{L < 0, L > -N\}$ is a 2-torus bundle over a 2-sphere with Chern class $(\omega_{\xi_N} - \omega_{\xi_L})/2$. Here ω is the standard volume form on the 2-sphere and ξ_N, ξ_L are the elements of \mathfrak{t} whose infinitesimal action is X_N and X_L , respectively.

Starting from the symplectic manifold \mathbb{R}^6 one can reduce with respect to the momentum K_m to obtain the manifold $M_k = K_m^{-1}(k)/S^1$. On M_k there is a (residual) circle action with momentum \bar{L} . The image of the (residual) momentum map is the intersection of the line $L_m = \{(m+1)N + (m-1)L = k\}$ with the image of the momentum map of the T^2 action.

We can now use the Duistermaat–Heckman theorem to compute the change in the (cohomology class of the) symplectic structure of the \bar{L} -reduced manifolds $M_{k,l} = \bar{L}^{-1}(l)/S^1$, and plot it as a function of l . The line L_m is spanned by the element $b = \xi_N^* - (m+1)/(m-1)\xi_L^*$. The cohomology class $\langle b, c \rangle$ is $\omega/(m+1)$ in the segment $L_m \cap E^+$ and $-\omega/(m+1)$ in the segment $L_m \cap E^-$. This gives, as expected, the graphs in Fig. 1.

III. QUANTUM SPECTRUM: LATTICE OF QUANTUM STATES

Given a 3D quantum diagram, an important problem is to “smoothly” map it to the lattice \mathbb{Z}^3 in \mathbb{R}^3 . This can always be done locally by means of independent local quantum numbers. In systems with nontrivial monodromy a global labeling of the eigenstates is impossible. To be more precise, a global labeling of the quantum states with three suitable global quantum numbers is the quantum analogue of the classical problem of defining global action functions for a completely integrable system. This problem has been shown to have no solution in systems with monodromy.²¹ The quantum numbers n_N and n_L are *a priori* global, because they correspond to global classical actions. On the other hand, because of the nontrivial classical monodromy of the swing spring system, the quantum number n_S can be only locally defined. In this section we show that this last quantum number cannot be defined globally, and we analyze this phenomenon.

Informally speaking, we try to construct a third global quantum number for the quantum swing spring, which is independent of n_L and n_N . Having three global quantum numbers corresponds to defining a bijection of the given lattice to the standard \mathbb{Z}^3 . Of course, many such bijections exist, but none of them can have the property of “ \hbar -smoothness,” which we define in Sec. III B. We begin by describing the quantum lattice of the quantum swing spring and then apply the idea of \hbar -smoothness.

A. Qualitative and quantitative description of the quantum lattice

One way of describing the 3D lattice of the quantum swing spring is to look at its planar slices, that is, the slices obtained by fixing a quantum number (n_N or n_{K_m} in our case). These plane slices intersect the thread of classical singular values (see Appendix A 3) in one point, which we refer to as a *singularity* of the quantum lattice.

To start with, we use the symmetries and the number of states discussed in Lemma 1 to deduce the qualitative aspects of the quantum spectrum of the swing spring. At the end of this section we give numerically computed pictures of the plane slices obtained by fixing the value of the polyad number n_N .

Let us now fix the polyad number n_N and then compute the joint spectrum of the operators \hat{L} and \hat{S} . We recall that the quantum spectrum one computes in this way is that of the classical system obtained from the original one by reducing it with respect to the circle action having momentum N at the value $n_N + 2$.

Lemma 2: For fixed polyad number n_N , the structure of the joint spectrum for the operators \hat{L} and \hat{S} is invariant under the symmetries $n_L \rightarrow -n_L$ and $n_S \rightarrow -n_S$ and it consists of four possible arrangements in a neighborhood of the intersection of the symmetry axes. These arrangements have a modulo 4 periodicity, $n_N \equiv n'_N \pmod{4}$, see Fig. 2.

From the symmetry σ_v and the pseudosymmetry discussed in Sec. II C, it follows that if (n_N, n_L, n_S) is a point of the quantum diagram, then also the points $(n_N, \pm n_L, \pm n_S)$ belong to the quantum spectrum.

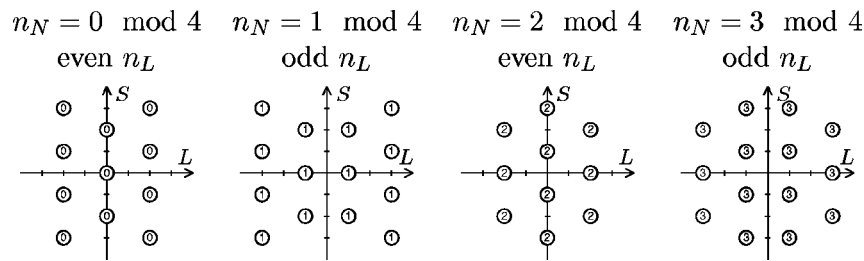


FIG. 2. Joint eigenvalues of the operators \hat{L} and \hat{S} near the origin.

Let us make the generic assumption that the spectrum of \hat{S} at fixed n_L has no degeneracies, that is, the spectrum of \hat{S} at fixed polyad numbers n_N and quantum number n_L is simple, and that the distances of consecutive \hat{S} -eigenvalues varies monotonically and slowly. In the rest of our argument we simply fix such distance to be some positive constant, say 2, as we did in the pictures in Fig. 2.

By Lemma 1, the quantum numbers n_N and n_L are both even or both odd, and when n_N is fixed n_L changes in steps of two. For even n_N , we have one central string of lattice points at $n_L=0$ with the maximum number of states $\mathcal{N}(n_N, n_L) = \frac{1}{2}n_N + 1$ for given n_N . This string is symmetric under $S \rightarrow -S$. For $n_N=0 \pmod 4$ it has the central node at $(0,0)$ because $\mathcal{N}(0 \pmod 4, 0)$ is odd. For $n_N=0 \pmod 2$ the closest to $(0,0)$ is a pair of nodes $(0, \pm 1)$ symmetric under $S \rightarrow -S$. Patterns for the other values of n_N are deduced by a similar argument. The other symmetric distributions are not admissible because they do not give the right rate of change of the number of quantum states as a function of n_L .

Corollary 1: For sufficiently small polyad numbers n_N , the quantum spectrum of the N -reduced normalized swing spring $(\hat{H}_{\text{nf}}^{(6)}, \hat{L})$ is qualitatively the same as the quantum spectrum of (\hat{S}, \hat{L}) in Lemma 2. Hence, the quantum diagrams of such systems are qualitatively the same as those in Fig. 2.

Figure 3 and, respectively, Fig. 4 display the joint spectrum of the operators \hat{L} and the Hamiltonian $\hat{H}_{\text{nf}}^{(6)}$, respectively, $\hat{H}_{\text{nf}}^{(3)}$, computed numerically for fixed polyad number n_N , and,

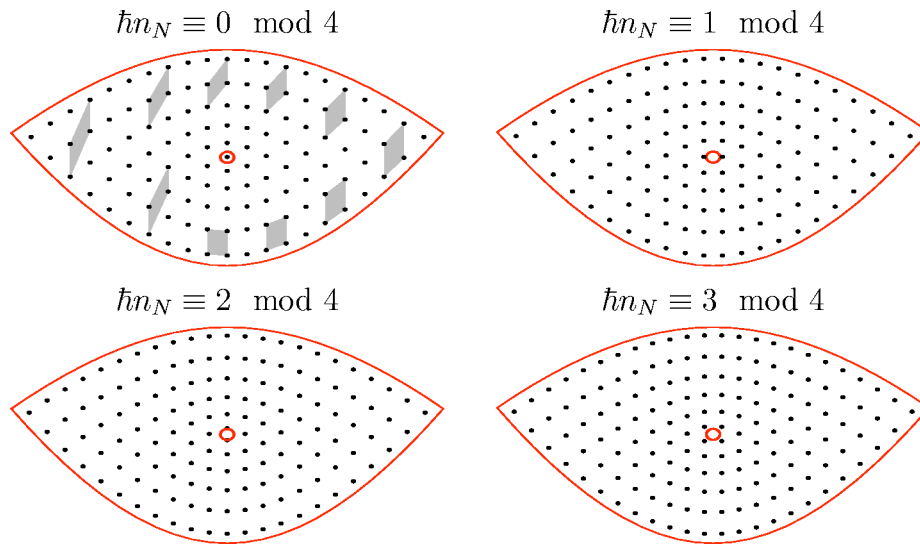


FIG. 3. Consecutive slices with fixed n_N polyad number for the normalized swing spring $(\hat{H}_{\text{nf}}^{(6)}, \hat{N}, \hat{L})$. The polyad quantum number n_N/\hbar is chosen to be about 1. Here \hbar is $1/20$.

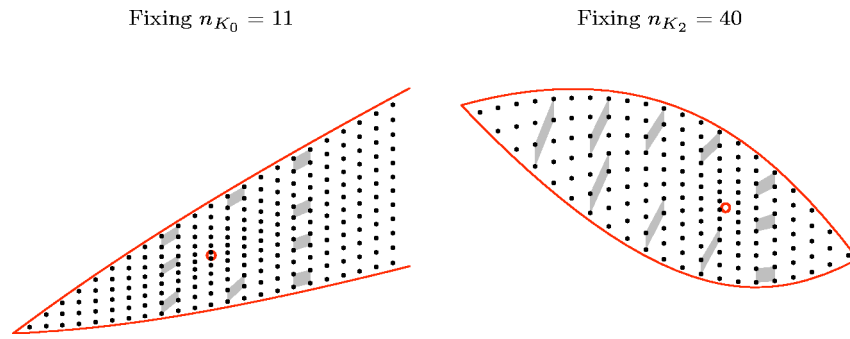


FIG. 4. Quantum diagrams obtained by fixing the quantum number n_{K_m} and plotting the quantum spectrum of the operators \hat{L} and $\hat{H}_{mf}^{(3)}$.

respectively, n_{K_0} and n_{K_2} . Note that, to preserve the qualitative structure of the approximating normalized system, one must choose a polyad number of the order of unity. With such a low polyad number there are too few quantum states to perform the analysis we are presenting here. A standard technique to increase the number of points in the quantum lattice (that is, states of the quantum system) at a fixed energy level is to scale the variables by the number $\sqrt{\hbar}$, where \hbar is the inverse of a natural number. This is equivalent to considering a Hilbert space of quantum states of the form $|n_1, n_2, n_3\rangle$ where n_i is a \hbar -multiple of a natural number.

In Sec. II D we gave a formula for the dependence on n_L of the number of quantum states having a fixed n_{K_m} quantum number. The results shown in Figs. 3 and 4 confirm the predictions made in Fig. 1 and used in Lemma 1.

B. Local mapping to the regular lattice

The effect of monodromy: Having described the plane slices and their relative position in 3-space, we can proceed with a tentative definition of the missing quantum number. Let us do this for the planar slices in Fig. 3. For every choice of quantum numbers n_N and n_L , that is, fixing the eigenspace associated to the quantum numbers n_N and n_L , one can assign a third quantum number by enumerating the quantum states of the operator \hat{S} in the joint eigenspace (n_N, n_L) , beginning with 0. Though this seems to be a global choice of third quantum number, we can easily show that it is not the case. As first suggested in Ref. 25, we can choose an elementary cell of the lattice and transport it around the classical singularity, see Fig. 3 (top left). After one tour around the singularity, we will come back with a different cell. This signifies that the third quantum number cannot be globally chosen.

Furthermore, when one fixes n_N and n_L and draws the curves having fixed the third quantum number proposed above, see Fig. 5, it is quite obvious that the curves above the classical singularity have a nonsmooth behavior, unlike those below. The closer \hbar is to zero, the more obvious

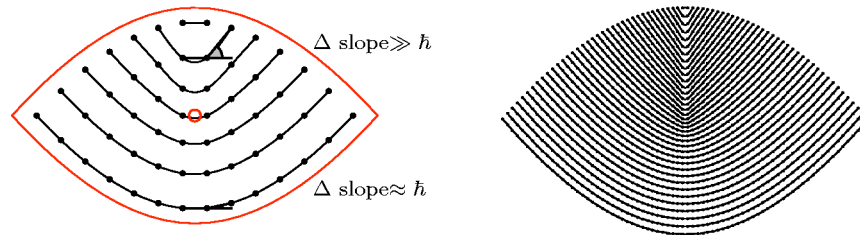


FIG. 5. Numbering the eigenstates with fixed n_L in the natural way within one n_N polyad of the system (S, L, N) . The curves connecting the eigenstates with the same label are not \hbar -smooth at $n_L=0$ and $S>0$. The classical singularity at $L=S=0$ is shown by an empty circle.

the discontinuity (or “kink”) in the tangent to the level curve becomes. Of course if one starts numbering from the top, one observes a nonsmooth behavior in the lines below the singularity. For this reason we introduce the following.

Definition 2: For a planar diagram, the choice of quantum numbers is \hbar -smooth if the discrete directional derivatives of the level curves obtained by fixing one quantum number are continuous of order \hbar . By *continuous of order \hbar* we mean that the difference of the discrete directional derivatives computed at two consecutive points must be of order of \hbar . An \hbar -smooth chart is a choice of \hbar -smooth quantum numbers. An \hbar -smooth atlas is a family of \hbar -smooth charts that cover $U_{\text{reg}} \subset U \subset \mathbb{R}^3$, the set of regular values in the image of the energy-momentum map.

The above definitions are void for a choice of \hbar of order 1. In fact, such a choice gives a quantum diagram with very few points, which makes every choice of quantum numbers \hbar -smooth. On the other hand, the nonexistence of global action variables implies that somewhere the level curves have a nonsmooth behavior of order one, which becomes visible when \hbar is sufficiently small, see Fig. 5.

The problem in numbering the quantum states is a consequence of a well-known obstruction to existence of classical global action variables known as *monodromy*.⁹ Monodromy is due to the nontriviality of the covering of U_{reg} defined by the period lattices. When the fundamental group of U_{reg} is \mathbb{Z} , the monodromy can be written as a matrix, which is called *monodromy matrix*. The inverse transpose of the monodromy matrix can be effectively computed by analyzing the quantum spectrum corresponding to the classical completely integrable system.^{12,23} The way we propose to do this is to use \hbar -smooth charts as follows. Let us cover the quantum lattice in U_{reg} (see Fig. 5) with two overlapping \hbar -smooth charts: one obtained by numbering the points in the columns starting from the bottom and the other obtained by numbering the points in the columns starting from the top. Let us choose in the first chart an *elementary cell*, which is a quadrangle that does not contain any lattice point in its interior or on its sides, with a distinguished vertex and an ordering of the sides adjacent to that vertex. Let us finally move the elementary cell in the first chart of the atlas following the level lines of the \hbar -smooth variables. Choosing a path that winds around the singular point and transporting our elementary cell along this path, one is forced, once the first region of chart overlap is reached, to identify the elementary cell with its corresponding representation in the second chart. Then one continues with the transport in the second chart. Reaching the second region of chart overlap, the elementary cell is identified with its representation in the first chart and then is compared with the initial cell. This final cell is *different* from the original one.

Definition 3: Given a n -dimensional quantum diagram admitting an \hbar -smooth atlas, an initial elementary cell defines a frame. The matrix expressing the change of frame from the initial elementary cell and the final elementary cell is the *quantum monodromy matrix*. A quantum monodromy matrix always belongs to $SL(n, \mathbb{Z})$.

In our example in Fig. 3, the sides of the final elementary cell, written with respect to the sides of the initial elementary cell as *columns*, define the quantum monodromy matrix $\begin{pmatrix} 1 & 0 \\ 2 & 1 \end{pmatrix}$.

In the same way, we can also compute the quantum monodromy matrix for other slices of the 3D lattice. For the K_0 and K_2 slices in Fig. 4 we obtain the matrices $\begin{pmatrix} 1 & 0 \\ 1 & 1 \end{pmatrix}$ and $\begin{pmatrix} 1 & 0 \\ 3 & 1 \end{pmatrix}$, respectively. This shows that the 2D monodromy depends on the choice of the slices, and therefore we must study directly the 3D monodromy by transporting a 3D elementary cell.

In the problem under investigation, the mod 4 periodicity allows one to project four subsequent constant N slices of the lattice on the same plane, creating the regular grid in Fig. 6 (left). In this projected lattice we can draw elementary cells and move them around the singularity at the origin. Choosing the initial cell as in Fig. 6 (right) and moving it around the origin of the projected lattice, being careful to move every vertex of the cell by the same number of steps, we find that the full monodromy matrix for the 3D lattice with that choice of initial elementary cell is

$$\begin{pmatrix} 1 & 0 & 0 \\ 2 & 1 & -1 \\ 0 & 0 & 1 \end{pmatrix}.$$

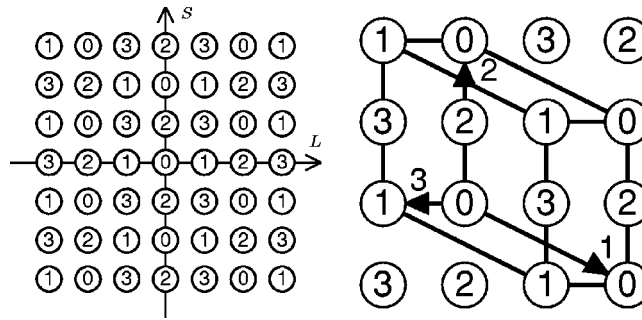


FIG. 6. Four n_N slices can be projected to the same plane, making it possible to draw and move an elementary cell. On the right, the choice of one such elementary cell. The numbers refer to the order of the sides.

IV. HOW TO OBTAIN THE 1:1:2 QUANTUM LATTICE FROM THE SIMPLE CUBIC LATTICE

A. 2D lemma and applications

Rather than using an \hbar -smooth atlas to compute the monodromy, one can introduce defects in regular lattices. The treatment we give here is inspired by Ref. 26.

Definition 4: Let (I_1, I_2) be coordinate functions on \mathbb{R}^2 . Let k be an integer. Consider the set $\mathcal{C}(kI_1: I_2) = \{(I_1, I_2) \in \mathbb{R}^2 \mid k|I_1| > 2|I_2|\}$, which we call a *wedge*. The set of points $\mathcal{D}(kI_1: I_2)$ in the complement of the wedge $\mathcal{C}(kI_1: I_2)$, after identifying the points with integral coordinates among those of the form $(n, nk/2) = (n, -nk/2)$ where $n \in \mathbb{Z}_{\geq 0}$, is called a *defect diagram*.

The above prescription can be easily adapted to the wedge $\mathcal{C}(kI_2: I_1) = \{(I_1, I_2) \in \mathbb{R}^2 \mid k|I_2| > 2|I_1|\}$.

Given a defect diagram associated to a wedge, the lattice obtained by vertically sliding the columns of lattice points, thus physically performing the identification, is called a *reconstructed diagram*, which we denote by $\mathcal{R}(kI_1: I_2)$. The process of taking a given lattice, introducing a cut and inserting or removing a wedge, is called *deconstruction of a diagram*. The vertex of the wedge is called a *defect point*. The defect point can be in any point of the $\{I_1, I_2\}$ plane.

Computing monodromy using a deconstructed diagram is straightforward. If we pick a square elementary cell below a wedge (assuming that k is positive) and translate it above the wedge, we end up with a parallelogram whose two sides remain orthogonal to the symmetry axis of the wedge, whereas the two other sides, initially parallel to the symmetry axis, have now slope k . This proves the following.

Lemma 3: The reconstructed diagram $\mathcal{R}(kI_1: I_2)$ has nontrivial monodromy. Its quantum monodromy matrix computed along a path winding counterclockwise around the origin, with respect to the elementary cell with vertex in $(0, -n)$ and with an ordered pair of sides $s_1 = [(0, -n), (1, -n)]$, $s_2 = [(0, -n), (0, -n+1)]$ is $\begin{pmatrix} 1 & 0 \\ k & 1 \end{pmatrix}$.

Remark 1: The monodromy matrix associated to a defect diagram depends solely on the type and position of the defect introduced and on the choice of the ordered sides of the elementary cell. It does not depend either on the path Γ one uses, or on the initial position of the vertex, nor on the point where Γ crosses the wedge. Also, the expression of the monodromy matrix M with respect to an arbitrary choice of elementary cell, whose defining frame $\{a_1, a_2\}$ gives the matrix $A \in \text{GL}(2, \mathbb{Z})$ with columns a_1 and a_2 , corresponds to the matrix $A^{-1}MA$.

It is straightforward to check that a clockwise rotation around the defect point changes the sign of k in the monodromy matrix while the monodromy matrix associated to the defect $\mathcal{R}(kI_2: I_1)$ is the matrix $\begin{pmatrix} 1 & -k \\ 0 & 1 \end{pmatrix}$.

Lemma 4: Suppose that the path Γ crosses a finite number of removed wedges in the order $\mathcal{C}_1, \dots, \mathcal{C}_n$. Then the monodromy matrix associated to this defect diagram computed along Γ is the matrix $M = M_{\mathcal{C}_n} \cdots M_{\mathcal{C}_1}$.

Proof: Choose the initial elementary cell. After crossing the first elementary wedge \mathcal{C}_1 , we

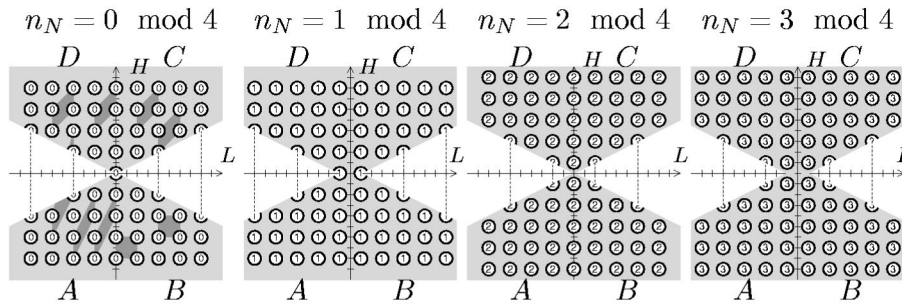


FIG. 7. Deconstruction of the diagrams obtained for constant n_N slices of the swing spring quantum diagram. Gluing the pictures along the dashed vertical lines one obtains the diagrams in Fig. 3.

obtain a cell which is formed by applying the matrix M_1 to the frame defining the initial elementary cell. By remark 1, crossing the second wedge C_2 produces a cell whose sides are identified by the columns of the matrix M_2M_1 . This argument is repeated until the last wedge has been passed and the lemma follows. \square

It is now time to apply the ideas above to the planar quantum diagrams in Figs. 3 and 4. The quantum diagrams in Fig. 3 have a nontrivial singularity at $(n_L, n_H) = (0, 0)$. Each of them can be deconstructed by introducing the two wedges $C(L:H)$ and $C(-L:H)$ as shown in Fig. 7. To keep the mod 4 period symmetries, one must choose a regular lattice with a step of 2 in the L direction and with order 2 period in the H direction. This is equivalent to placing the defect point not at the origin of a regular lattice. The monodromy matrix computed using Lemma 3 is precisely the one obtained using \hbar -smooth charts in Figs. 3 and 4.

The two planar quantum diagrams in Fig. 4 can be treated in a similar way and give the deconstructed diagrams in Fig. 8. From these diagrams we find that the quantum monodromy matrix for slices with constant quantum number n_{K_m} is $\begin{pmatrix} 1 & 0 \\ m+1 & 1 \end{pmatrix}$.

B. 3D lemma and applications

We now extend the idea of a defect diagram in order to deconstruct the 3D quantum diagram of the swing spring. It is natural to define a defect of a three-dimensional regular lattice by extending a defect of a two-dimensional lattice trivially in one direction.

Definition 5: Let (I_1, I_2, I_3) be coordinate functions on \mathbb{R}^3 . A two-dimensional wedge $C(kI_1:I_2)$ can be trivially extended along the direction I_3 , meaning that all constant I_3 slices intersect this extension in the same wedge. Such a 3D wedge is *trivial in the I_3 direction* and is denoted by $C(kI_1:I_2:I_3)$.

The boundary of the 3D wedge $C(kI_1:I_2:I_3)$ consists of a roof made up of two half-planes joined along the I_3 axis, which is a “roof top.” The roof top is a singularity of the 3D quantum diagram called *defect line*.

Lemma 5: The reconstructed diagram $\mathcal{R}(kI_1:I_2:I_3)$ has nontrivial monodromy. Its quantum monodromy matrix computed along a path winding counterclockwise in the $\{I_1, I_2\}$ plane around the positively oriented defect line, the I_3 axis, with respect to the elementary cell with vertex in

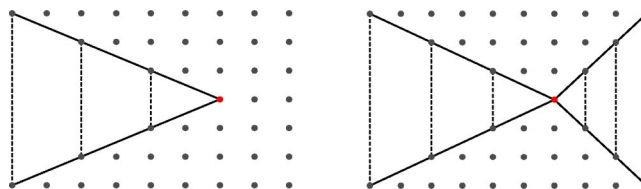


FIG. 8. Deconstructed n_{K_0} and n_{K_2} slices.

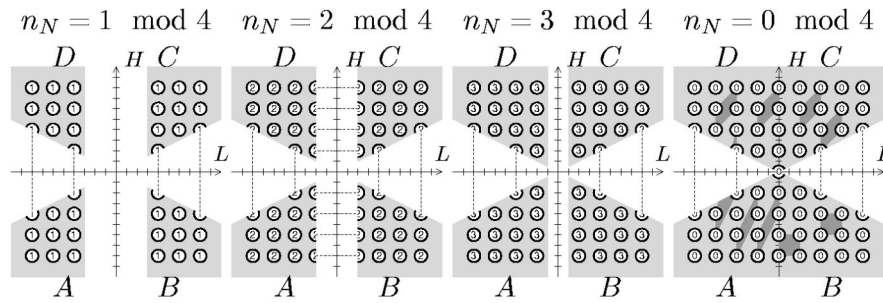


FIG. 9. Defect for constant n_N slices of the joint spectrum of the quantum swing spring. The slices with nonzero $n_N \bmod 4$ are obtained from the $n_N=0 \bmod 4$ lattice by cutting out an additional region along the vertical axis. Dashed vertical lines show identification of points on the border of the cutout regions.

$(0, -n, 0)$ and with sides $s_1=[(0, -n, 0), (1, -n, 0)]$, $s_2=[(0, -n, 0), (0, -n+1, 0)]$, $s_3=[(0, -n, 0), (0, -n, 1)]$ is the matrix

$$\begin{pmatrix} 1 & 0 & 0 \\ k & 1 & 0 \\ 0 & 0 & 1 \end{pmatrix}.$$

When a path crosses a family of 3D wedges, the monodromy matrix along the path is obtained as in Lemma 4.

Again, one must be careful when treating a defect with a different orientation. Let us choose, say $\mathcal{D}(kI_3:I_1:I_2)$. A path winding counterclockwise in the $\{I_3, I_1\}$ plane is a path which begins at the positive I_3 axis and moves towards the positive I_1 axis. The monodromy matrix for the elementary cell in lemma 5 along such path is the matrix

$$\begin{pmatrix} 1 & 0 & k \\ 0 & 1 & 0 \\ 0 & 0 & 1 \end{pmatrix}.$$

The diagrams in Fig. 7, which are obtained for fixed polyad number n_N , can be modified by introducing auxiliary spacings along the vertical axis S as shown in Fig. 9. Though inessential in the planar figures, this modification helps to deconstruct the 3D lattice of the quantum swing spring up to any fixed polyad number N_{\max} into a regular cubic lattice with three 3D wedges removed, namely, $\mathcal{C}(L:H:N)$, $\mathcal{C}(-L:H:N)$, and $\mathcal{C}(-N:L:H)_{(0,0,N_{\max})}$, see Fig. 10. The roof tops of the first two 3D wedges lie on the N axis, which is the singular thread of the energy momentum

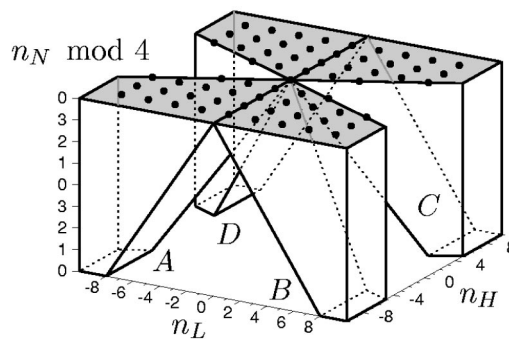


FIG. 10. Three-dimensional model of the deconstructed joint spectrum of the quantum swing spring.

map \mathcal{EM} of the classical swing spring. The roof top of the last 3D wedge lies on the line $\{L=0, N=N_{\max}\}$. This last singular line should be pushed at infinity to obtain the quantum diagram of the swing spring.

The pictures in Fig. 7 account for the 2D wedges of the 3D wedge $\mathcal{C}(\pm L:H:N)$; the cut along the H axis shown in Fig. 9 corresponds to the 3D wedge $\mathcal{C}(-N:L:H)_{(0,0,N_{\max})}$. The deconstruction of the swing spring quantum lattice resembles a table with four legs, labeled by $A \subset \{n_H < 0, n_L < 0\}$, $B \subset \{n_H < 0, n_L > 0\}$, $C \subset \{n_H > 0, n_L > 0\}$, and $D \subset \{n_H > 0, n_L < 0\}$ as shown in Fig. 10.

V. CALCULATION OF MONODROMY USING SIMPLE CUBIC LATTICE WITH CUTS

In this section we use the deconstructed 3D quantum lattice of the swing spring in the preceding section to calculate the monodromy matrix associated to a path winding around the defect line situated on the vertical N axis.

Let us start the path in the component A of Fig. 10 and move counterclockwise around the defect line. Passing from A to B , we cross the elementary wedge $\mathcal{C}(-N:L:H)_{(0,0,N_{\max})}$. In passing from B to C we cross the elementary wedge $\mathcal{C}(L:H:N)$. In passing from C to D we cross again the elementary wedge $\mathcal{C}(-N:L:H)_{(0,0,N_{\max})}$. Returning to the component A we cross the elementary wedge $\mathcal{C}(-L:H:N)$. From Lemma 5 it follows that the quantum monodromy matrix of the quantum swing spring along the given path is

$$M = \begin{pmatrix} 1 & 0 & 0 \\ 1 & 1 & 0 \\ 0 & 0 & 1 \end{pmatrix} \begin{pmatrix} 1 & 0 & 1 \\ 0 & 1 & 0 \\ 0 & 0 & 1 \end{pmatrix} \begin{pmatrix} 1 & 0 & 0 \\ 1 & 1 & 0 \\ 0 & 0 & 1 \end{pmatrix} \begin{pmatrix} 1 & 0 & 1 \\ 0 & 1 & 0 \\ 0 & 0 & 1 \end{pmatrix}^{-1} = \begin{pmatrix} 1 & 0 & 0 \\ 2 & 1 & -1 \\ 0 & 0 & 1 \end{pmatrix}.$$

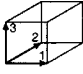
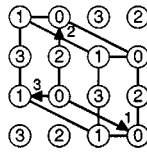
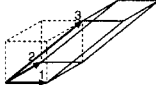
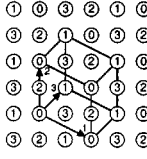
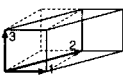
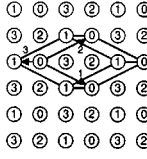
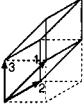
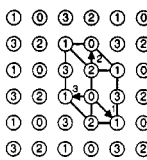
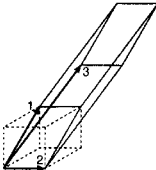
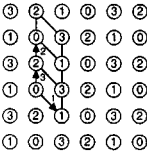
The matrix M above is expressed with respect to a frame determined by the initial unitary cubic elementary cell. This implies that with a different choice of elementary cell one would obtain a new quantum monodromy matrix related to M by conjugation in $SL(3, \mathbb{Z})$.

It is therefore natural to try to determine an initial elementary cell for which the monodromy matrix assumes its simplest form. In the discussion above we choose an initial cell, labeled α in Table I, and then we compute the monodromy associated to this cell. We now take five different cells in quadrant A of the lattice, namely, $\alpha, \beta, \gamma, \delta$, and κ , as shown in Table I. We denote by $\{a_1, a_2, a_3\}$ the frame associated to the cell α , the frames associated to the cells β, γ, δ , and κ , are $\{b_1, b_2, b_3\}$, $\{c_1, c_2, c_3\}$, $\{d_1, d_2, d_3\}$, and $\{k_1, k_2, k_3\}$, respectively. They are related to the frame defining α by the matrix given in the second column of Table I.

Once we have embedded each elementary cell in the component A of the deconstructed diagram of Fig. 10 or in the projected diagram of Fig. 9, we can move it around the vertical defect corresponding to the singular thread of the energy momentum map of the classical swing spring, and compute the quantum monodromy matrix. From Table I we see that the monodromy matrix of the quantum diagram of the swing spring system takes the simplest possible form of a unipotent matrix with only one nonzero off-diagonal entry equal to 1, when κ is chosen as initial elementary cell.

Observe that for 3D quantum diagrams the sign is not an invariant as it is for the 2D quantum diagrams, see Ref. 7. More specifically, the monodromy matrix of all 2D quantum diagrams, associated to a two degree of freedom completely integrable Hamiltonian system with a circle symmetry, have the form $\begin{pmatrix} 1 & 0 \\ k & 1 \end{pmatrix}$ with $k > 0$. Such matrices can be obtained by introducing the 2D defects we gave above. Another 2D defect obtained by adding a solid wedge instead of subtracting it produces a minus sign in the monodromy matrix $\begin{pmatrix} 1 & 0 \\ -k & 1 \end{pmatrix}$. The two matrices are not conjugate in $SL(2, \mathbb{Z})$. At the same time, when the dimension is bigger than 2 such sign can be changed by conjugation in $SL(3, \mathbb{Z})$. So, while the construction of defects by removing and adding solid wedges still exists in 3D, the monodromy matrix cannot distinguish them.

TABLE I. Possible choices of elementary cells in the unit cell basis of the reconstructed \mathcal{EM} lattice of quantum swing spring.

Cell	A	Shape	Shape ^a	$A^{-1} M A$
α	$\begin{pmatrix} 1 & 0 & 0 \\ 0 & 1 & 0 \\ 0 & 0 & 1 \end{pmatrix}$			$\begin{pmatrix} 1 & 0 & 0 \\ 2 & 1 & -1 \\ 0 & 0 & 1 \end{pmatrix} = M$
β	$\begin{pmatrix} 1 & 0 & 1 \\ 0 & 1 & 1 \\ 0 & 0 & 1 \end{pmatrix}$			$\begin{pmatrix} 1 & 0 & 0 \\ 2 & 1 & 1 \\ 0 & 0 & 1 \end{pmatrix}$
γ	$\begin{pmatrix} 1 & 1 & 0 \\ 0 & 1 & 0 \\ 0 & 0 & 1 \end{pmatrix}$			$\begin{pmatrix} -1 & -2 & 1 \\ 2 & 3 & -1 \\ 0 & 0 & 1 \end{pmatrix}$
δ	$\begin{pmatrix} 1 & 0 & 0 \\ 0 & 1 & 0 \\ 1 & 0 & 1 \end{pmatrix}$			$\begin{pmatrix} 1 & 0 & 0 \\ 1 & 1 & -1 \\ 0 & 0 & 1 \end{pmatrix}$
κ	$\begin{pmatrix} 1 & 0 & 1 \\ 0 & 1 & 1 \\ 1 & 0 & 2 \end{pmatrix}$			$\begin{pmatrix} 1 & 0 & 0 \\ 1 & 1 & 0 \\ 0 & 0 & 1 \end{pmatrix}$

^aPossible choices of elementary cells in the A quadrant of the initial 3D quantum diagram.

VI. COMPARISON OF CLASSICAL AND QUANTUM CALCULATIONS OF MONODROMY

We now recall how the classical monodromy matrix of the swing spring was computed in Ref. 11. Define the momenta $N_1=(N+L)/2$ and $N_2=(N-L)/2$. Fixing the values of the momenta and of the energy, one specifies a 3-torus. It is possible to define a basis of the fundamental group of this torus by means of three paths generated as follows: $\gamma_{N_1}=\exp(tX_{N_1})$, $\gamma_{N_2}=\exp(tX_{N_2})$, and

$$\gamma_H = \exp \frac{t}{2\pi} (TX_H - \Theta_1 X_{N_1} - \Theta_2 X_{N_2}).$$

Here Θ_1 and Θ_2 are the rotation numbers of the flow of X_H on the given 3-torus and T is its fully reduced period, see Ref. 11. Considering the initial choice of three paths as a frame, and then moving the paths around the singular thread with a continuous homotopy (imposed by the functions T, Θ_1, Θ_2) one ends up with three final paths, or final frame. The matrix of change of frames is the classical monodromy matrix of the swing spring and is

$$\begin{pmatrix} 1 & 0 & 0 \\ 0 & 1 & 0 \\ 1 & -1 & 1 \end{pmatrix}.$$

Observe that K_m (7) and L are not the momenta of an effective 2-torus action. In fact L is the momentum of the $-1:1:0$ oscillator; while K_m is the momentum of the $1:m:m+1$ oscillator. Thus the momentum K_m+L is that of the $0:m+1:m+1$ oscillator, whose flow is $2\pi/(m+1)$ periodic. Despite this noneffectiveness, one can show that the classical monodromy matrix with respect to the frame $\gamma_L = -\gamma_{N_1} + \gamma_{N_2}$, $\gamma_{K_m} = \gamma_{N_1} + m\gamma_{N_2}$, and γ_H is

$$\begin{pmatrix} 1 & 0 & 0 \\ 0 & 1 & 1 \\ 0 & 0 & 1 \end{pmatrix}.$$

Reducing with respect to the circle action with momentum K_m one obtains a 2D system whose monodromy is represented by the matrix $\begin{pmatrix} 1 & 1 \\ 0 & 1 \end{pmatrix}$. At first sight this does not seem to be in agreement with the quantum results computed when n_{K_m} is held constant. However, one observes that the noneffectiveness of the T^2 action generated by the flows of X_{K_m} and X_L implies that a basis of cycles in the 2-tori of the K_m -reduced space are not the cycles $\tilde{\gamma}_L$ and $\tilde{\gamma}_H$, where the tildes represent the projection of γ_L and γ_N on the reduced space, but the cycles $\tilde{\gamma}_L/(m+1)$ and $\tilde{\gamma}_H$. With respect to these cycles the monodromy matrix is the matrix $\begin{pmatrix} 1 & m+1 \\ 0 & 1 \end{pmatrix}$, which confirms our quantum calculations.

Another interesting aspect of the 2D system, highlighted by reduction of the symmetry associated to the K_m momentum, is that the singular fiber of the energy momentum map of the reduced completely integrable system is always a singly pinched torus. This does not contradict the monodromy theorem in Refs. 6 and 27. In fact, the phase space of the 2D system obtained by K_m reduction is *not* smooth, being singular precisely at the pinch point of the singular fiber of its energy momentum mapping. Consequently, this pinch point is not a focus–focus critical point.

To find the relation between the quantum monodromy matrices and the classical monodromy matrix we follow Appendix A 2 in Ref. 12 and choose the elementary cell whose sides in the space with coordinates (N_1, N_2, H) are given by the vectors $e_1 = (1, 0, \Theta_1/T)$, $e_2 = (0, 1, \Theta_2/T)$, and $e_3 = (0, 1/T, 0)$, where $\Theta = (\Theta_1 + \Theta_2)/2$. Mapped onto (L, H, N) -space these vectors become $f_1 = (1, \Theta_1/T, 1)$, $f_2 = (-1, \Theta_2/T, 1)$, and $f_3 = (0, 1/T, 0)$. Computing the values Θ_1 and Θ_2 after completing a circuit, one finds that the cell is precisely the one called γ in Table I (up to exchanging e_2 and e_3). The quantum matrix associated to this cell is

$$\begin{pmatrix} 1 & 0 & 0 \\ 0 & 1 & 0 \\ 1 & -1 & 1 \end{pmatrix},$$

which is precisely the inverse transpose of the classical monodromy matrix.

VII. CONCLUSIONS

In this paper, we have analyzed the qualitative features of a model quantum system with 3 degrees of freedom whose classical limit corresponds to an integrable approximation of a swing spring in 1:1:2 resonance.

Quantum monodromy is manifested in the joint spectrum of three commuting observables. Locally, this joint quantum spectrum can almost everywhere be interpreted as a regular lattice of quantum states. This reflects the existence of local action variables in the corresponding classical system. Equivalently, the joint spectrum can be described globally as a regular lattice of quantum states with defects. Thus it is clear that quantum and classical monodromy are directly related. The atlas formed by different \hbar -smooth local charts covers almost all the quantum lattice with the exception of regions containing nonregular values of the classical energy momentum map. Quantum monodromy can be directly read from the joint spectrum by looking at the evolution of an elementary cell of the quantum lattice along a closed path lying in \hbar -smooth charts of an \hbar -smooth atlas of the lattice.

Globally the 3D quantum lattice is interpreted as a regular lattice with 1D defects. The construction of 1D defects for 3D lattices, which are characterized by the elementary monodromy matrix, follows the recipe formulated for 2D lattices with point defects which are obtained by cutting out a wedge from the regular lattice and gluing together the boundaries which have been created. For the 1:1:2 swing spring we have shown that the lattice of quantum states can be reconstructed from a regular cubic lattice by removing three solid wedges, two of which create a line defect in the physical region while the third creates a line defect, which lies in a nonphysical region at infinity. The representation of the 3D quantum lattice of the swing spring by a simple cubic lattice with wedges removed allows us to visualize clearly the transport of the elementary cell over the lattice. It also allows us to calculate the matrix of quantum monodromy for any choice of initial elementary cell in the lattice.

An important additional consequence of our analysis of the quantum swing spring is the clear demonstration that 1D defects in the 3D lattice (or equivalently 1D subspaces of critical values of the 3D classical energy-momentum map) should be characterized by the complete 3D quantum/classical monodromy matrix. The analysis of two-dimensional slices is *insufficient* to uncover the singularities of the full 3D quantum lattice. Therefore it is important to be able to understand the geometry of lattices of any dimension and be able to compute its quantum monodromy as a transformation of an elementary cell along a close path. Deconstruction/reconstruction of lattices seems to be an essential tool in the analysis of quantum lattices and in the computation of their quantum monodromy. It is an open question whether 3D quantum lattices exist whose monodromy cannot be reproduced via the introduction of elementary defects. In 2D we know how to decompose any quantum monodromy matrix into a product of elementary matrices. Therefore every defect of a 2D quantum lattice arises from a known set of elementary defects, see Ref. 8.

Monodromy of n -dimensional lattices is defined up to conjugation in $SL(n, \mathbb{Z})$. In particular, it cannot distinguish between two different defects obtained by removing or adding the same angular part in a regular lattice. Whether the defect corresponding to adding a wedgelike region to a regular lattice can be realized by an integrable Hamiltonian system is an open question. The 1D lattice defects in 3D systems introduced here straightforwardly generalize to codimension 2 defects in integrable Hamiltonian systems with arbitrary number of degrees of freedom. Codimension 1 defects which correspond to fractional monodromy²² can also be treated with the same approach. It is worth noting that the whole 3D quantum lattice of the quantum swing spring, has a defect of codimension 2 which corresponds to integer monodromy, even though the 1:1:2 system studied in this paper has a 1:2 resonant subsystem with a fractional defect.¹ In order to see codimension 1 defects and fractional monodromy for 3D quantum lattices, we need to study more complicated examples of integrable Hamiltonian systems with higher order resonances.

ACKNOWLEDGMENT

During the preparation of this paper the authors were supported by the EU project HPRN-CT-2000-0113 *MASIE—Mechanics and Symmetry in Europe*.

APPENDIX A: REDUCTION OF RESONANT OSCILLATOR SYSTEMS IN THREE DIMENSIONS WITH $SO(2)$ SYMMETRY

Consider an $m' : m' : m''$ resonant 3-oscillator system with zero order Hamiltonian

$$H_0 = m' \frac{1}{2}(z_1 \bar{z}_1) + m' \frac{1}{2}(z_2 \bar{z}_2) + m'' \frac{1}{2}(z_3 \bar{z}_3) \quad (\text{A1})$$

and whose higher order terms Poisson commute with H_0 . Here the positive integer numbers m' and m'' are such that $\gcd(m', m'') = 1$, and (z, \bar{z}) are complex symplectic coordinates of the form $(q \pm ip)$. The flow of H_0 generates an oscillator symmetry S^1 whose action on the six dynamical variables $(z_1, z_2, z_3, \bar{z}_1, \bar{z}_2, \bar{z}_3)$ is given by the 6×6 diagonal matrix,

$$U_t = \text{diag}(e^{im't}, e^{im't}, e^{im''t}, e^{-im't}, e^{-im't}, e^{-im''t}) = \text{diag}(\theta^{m'}, \theta^{m'}, \theta^{m''}, \theta^{-m'}, \theta^{-m'}, \theta^{-m''}). \quad (\text{A2})$$

Suppose that this system is invariant with respect to the additional Lie symmetry group $\text{SO}(2)$ of rotations in the plane (z_1, z_2) , whose action is represented by the matrix

$$U_s = \text{diag}\left[\begin{pmatrix} \cos s & \sin s \\ -\sin s & \cos s \end{pmatrix}, 1, \begin{pmatrix} \cos s & \sin s \\ -\sin s & \cos s \end{pmatrix}, 1\right]. \quad (\text{A3})$$

It can be seen that the two actions (A3) and (A2) commute, and that the full symmetry group of such system is therefore a torus $T^2 = S^1 \times \text{SO}(2)$.

We study the case where $m' : m''$ is 1:2. The indices 1,2,3 of our coordinates here correspond to ξ, η, ζ in Sec. II A. In this appendix we give details of the reduction of the $S^1 \times \text{SO}(2)$ symmetry of this system. It can be considered as a two-stage reduction. For example, first we reduce the 3-oscillator symmetry and then the $\text{SO}(2)$ symmetry. We will do the two stages at once. Since the T^2 action is not free, we use *singular reduction*.³

We also consider certain discrete symmetries. It can be verified easily that the spatial symmetry of the spherical pendulum as well as that of the swing spring system¹¹ is not just the plain $\text{SO}(2)$ but the group $\text{SO}(2) \rtimes C_s$. Here $C_s = \{1, \sigma_v\}$ is the group of reflections in a plane containing the $\text{SO}(2)$ symmetry axis. Explicitly

$$\sigma_v: (q_1, q_2, q_3, p_1, p_2, p_3) \mapsto (q_2, q_1, q_3, p_2, p_1, p_3), \quad (\text{A4a})$$

where by convention we take q_3 as the symmetry axis.

The Schönflies notation for such group is $C_{\infty v}$. The total symmetry group of these systems is $\text{SO}(2) \rtimes C_s \times \mathcal{T}$ and combines the above spatial group with the antisymplectic momentum reversal symmetry,

$$\mathcal{T}: (q, p, z) \rightarrow (q, -p, \bar{z}), \quad (\text{A4b})$$

which is present in many other physical systems and is often called *time reversal*. So we will consider an additional discrete group of order four

$$\{1, \sigma_v, \mathcal{T}, \mathcal{T}_s = \mathcal{T} \circ \sigma_v\}$$

which is isomorphic as an abstract group to $\mathbb{Z}_2 \times \mathbb{Z}_2$.

1. Generating function and integrity basis

By Molien's theorem,²⁰ the generating function for the invariants of the $S^1 \times \text{SO}(2)$ action is given by the double integral,

$$g(\lambda) = \frac{1}{2\pi} \int_0^{2\pi} \frac{1}{2\pi} \int_0^{2\pi} \frac{1}{\det(1 - \lambda U_t U_s)} dt ds. \quad (\text{A5})$$

Here the formal variable λ represents any of the dynamical variables (z, \bar{z}) or, equivalently, (q, p) . In the complex unimodular variables

$$\theta = \exp(it) \quad \text{and} \quad \varphi = \exp(is)$$

the determinant in (A5) can be expressed as

$$\det(1 - \lambda U_t U_s) = (\lambda - \theta^2) \left(\lambda - \frac{1}{\theta^2}\right) (\lambda - \theta\varphi) \left(\lambda - \frac{1}{\varphi\theta}\right) \left(\lambda - \frac{\theta}{\varphi}\right) \left(\lambda - \frac{\varphi}{\theta}\right).$$

The generating function (A5) can now be computed as a double Cauchy integral,

$$g(\lambda) = \frac{1}{2\pi i} \oint_{|\theta|=1} \frac{1}{2\pi i} \oint_{|\varphi|=1} \frac{\lambda^2 \theta^3 \varphi d\theta d\varphi}{D(\theta, \varphi; \lambda)}, \tag{A6}$$

where

$$D(\theta, \varphi; \lambda) = (\lambda - \theta^2) \left(\theta^2 - \frac{1}{\lambda} \right) (\lambda - \theta\varphi) \left(\varphi\theta - \frac{1}{\lambda} \right) (\lambda\varphi - \theta)(\lambda\theta - \varphi).$$

Since the formal variable λ is used to Taylor expand $g(\lambda)$ at $\lambda=0$, it can be arbitrarily small. This means that when we integrate (A6) on θ we should consider only four poles,

$$\theta = \pm \sqrt{\lambda}, \quad \theta = \frac{\lambda}{\varphi}, \quad \theta = \lambda\varphi,$$

which lie inside the unit circle $|\theta|=1$. Applying the Cauchy integral formula for each pole and then integrating the result on φ in the similar way gives the Molien generating function,

$$g(\lambda) = \frac{1 + \lambda^3}{(1 - \lambda^2)^3(1 - \lambda^3)}. \tag{A7}$$

The function (A7) indicates not only the fact that the space of invariant polynomials is generated by *five* polynomials, three quadratic and two cubic, but also that this ring is not freely generated and that the integrity basis of this ring has four principal (denominator) invariants and one cubic auxiliary (numerator) invariant. From (A2) we see that all invariants of the 1:1:2 oscillator action are built from monomials $z_1\bar{z}_1, z_2\bar{z}_2, z_3\bar{z}_3, z_1\bar{z}_2, z_1^2\bar{z}_3, z_2^2\bar{z}_3, z_1z_2\bar{z}_3$ and their conjugates which should be further symmetrized with respect to the SO(2) action in (A3). The explicit choice of invariants is

$$N = \frac{1}{2}(z_1\bar{z}_1 + z_2\bar{z}_2 + 2z_3\bar{z}_3), \quad R = \frac{1}{2}(z_1\bar{z}_1 + z_2\bar{z}_2), \quad L = \Im(\bar{z}_1z_2),$$

$$S = \frac{1}{2}\Re(z_3(\bar{z}_1^2 + \bar{z}_2^2)), \quad T = \frac{1}{2}\Im(z_3(\bar{z}_1^2 + \bar{z}_2^2)).$$

In the rotated coordinates $q_1, q_2, q_3, p_1, p_2, p_3$ of Sec. II A these invariants equal those in (3). Comparing with Ref. 11 we find that

$$N = \frac{1}{2}\rho_1 + \frac{1}{2}\rho_2 + \rho_3, \quad R = \frac{1}{2}\rho_1 + \frac{1}{2}\rho_2, \quad S = -\rho_4, \quad T = \rho_5.$$

Note that coordinates ξ, η, ζ in Ref. 11 correspond to our rotated coordinates q_1, q_2, q_3 in Sec. II A. Choosing T to be the auxiliary invariant, we can represent the structure of the ring as

$$\mathbb{R}[N, R, L, S] \bullet \{1, T\} = \mathbb{R}[N, R, L, S] \oplus \mathbb{R}[N, R, L, S]T, \tag{A8}$$

where the ring $\mathbb{R}[N, R, L, S]$ is freely generated by (N, R, L, S) .

A different way to reflect the structure of the ring (A8) is by specifying the relations (*syzygies*) between its generators. Rewriting the function (A7) in the Hilbert form,

$$g(\lambda) = \frac{1 - \lambda^6}{(1 - \lambda^2)^3(1 - \lambda^3)^2}, \tag{A7a}$$

we see that there is one such relation of degree 6. From our choice of invariants (3) we find

$$2\Phi_{n,l}^{1:1:2} = T^2 + S^2 - (R - L)(R + L)(N - R) = 0, \tag{A9a}$$

and we can also verify that

$$N \geq R \geq |L| \geq 0. \tag{A9b}$$

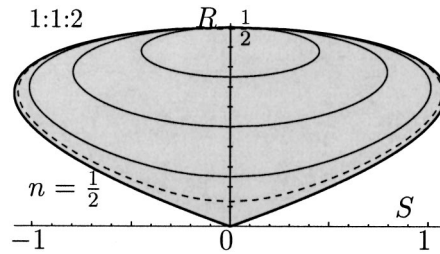


FIG. 11. Reduced phase space $P_{n,l}^{1:1:2}$ of the 1:1:2 resonant oscillator system with $SO(2)$ symmetry. Shaded area bounded by a bold line shows the projection of the singular space $P_{n,0}^{1:1:2}$ on the plane $\{T=0\}$; other lines show boundaries of similar projections for $l=\frac{1}{5}n$ (dashed line), $\frac{1}{4}n$, $\frac{1}{2}n$, and $\frac{3}{4}n$; note that $l_{\max}=n$.

2. Reduced space and Hamiltonian

From the preceding section it is obvious that the T^2 -reduced system (the doubly reduced system in Ref. 11) can be described in terms of invariants (R, S, T) . The space $L^{-1}(l) \cap N^{-1}(n)$ is to be reduced by the T^2 -action generated by the flows of X_L and X_N . Equation (A9a) defines the reduced phase space $P_{n,l}^{1:1:2}$, which is a surface of revolution about the R axis in the ambient 3-space with coordinate functions (R, S, T) . The projection of $P_{n,l}^{1:1:2}$ on the $\{T=0\}$ plane is shown in Fig. 11.

When $n=l=0$ or when $|l|=n$ the space $P_{n,l}^{1:1:2}$ degenerates to a point; for all $n > |l| \neq 0$ it is diffeomorphic to a 2-sphere. When $l=0$ and $n > 0$ the space $P_{n,0}^{1:1:2}$ is a sphere with one singular point at $R=S=T=0$ (a “turnip”). Since near this point $\rho^2 = T^2 + S^2 \approx nR^2$, the singularity is conical (as in the case of the 1:2 resonance).¹

The reconstruction of the T^2 orbit map $L^{-1}(l) \cap N^{-1}(n) \subset TR^3 \mapsto P_{n,l}^{1:1:2}$ can be described as follows. The two points $l = \pm n$ lift to two relative equilibria which correspond to pure (and fast) rotation about axis q_3 without swinging nor springing; of course the spring is stretched and the pendulum is somewhat bent. All points of $P_{n,l}^{1:1:2}$ with $0 < |l| < n$ lift to the regular T^2 orbits of the $S^1 \times SO(2)$ group with periods 2π in both directions. Same is true for all regular points of $P_{n,0}^{1:1:2}$, that is, all points with $R \neq 0$. The singular point of this space (with $S=R=0$) goes to a special periodic orbit in $L^{-1}(0) \cap N^{-1}(n)$ of period π . It corresponds to pure swinging along the q_3 axis.

The triple of Hamiltonian functions (R, S, T) generates the Poisson algebra of the (second) reduced system which defines the Poisson structure on $P_{n,l}^{1:1:2}$. Using the functions defined in (3), we compute this Poisson structure first in the original phase space TR^3 (note that $\{z, \bar{z}\} = 2i$), take (A9a) into account and restrict to $P_{n,l}^{1:1:2}$. This gives the structure

$$\{R, S\} = 2T, \quad \{T, R\} = 2S, \quad \{S, T\} = 3R^2 - 2nR - l^2. \quad (A10a)$$

The function (A9a) is the Casimir of this algebra and we can also see that

$$\{\psi_a, \psi_b\} = \sum_c \varepsilon_{abc} \frac{\partial \Phi_{n,l}^{1:1:2}}{\partial \psi_c}, \quad \text{where } \psi = (\psi_1, \psi_2, \psi_3) = (R, S, T). \quad (A10b)$$

Introducing a new set of functions

$$\mathfrak{N} = \frac{1}{4}(N - |L|), \quad \mathfrak{N}_1 = \frac{1}{2}R - \frac{1}{4}(N + |L|), \quad \mathfrak{N}_2 = S\chi^{-1}, \quad \mathfrak{N}_3 = T\chi^{-1}, \quad (A11a)$$

where

$$\chi = 2\sqrt{R + |L|} \quad \text{and} \quad \mathfrak{N}^2 = \mathfrak{N}_1^2 + \mathfrak{N}_2^2 + \mathfrak{N}_3^2, \quad (A11b)$$

deforms the Poisson algebra (A10) into a standard $so(3)$ algebra with generators $(\mathfrak{N}_1, \mathfrak{N}_2, \mathfrak{N}_3)$ and Casimir \mathfrak{N} . It follows that the singular map (A11) sends every reduced phase space $P_{n,l}^{1:1:2}$ to a smooth sphere S^2 of radius \mathfrak{N} (which is maximal when $l=0$ and zero when $|l|=l_{\max}=n$). The conelike singularity of $P_{n,0}^{1:1:2}$ at $n > 0$ is removed due to the singularity of this map at $R=L=0$.

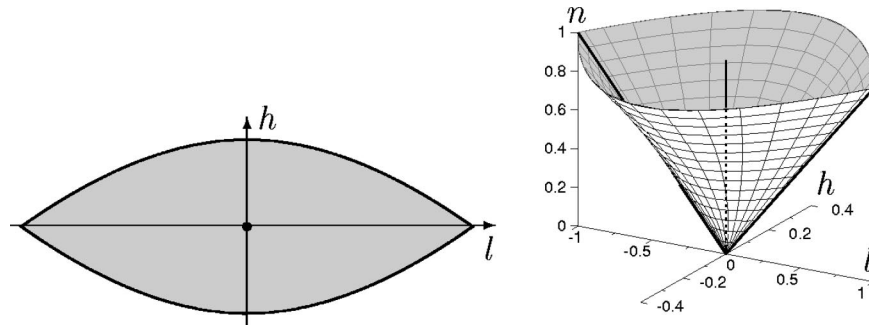


FIG. 12. Constant $n > 0$ slice (left) of the image of the energy-momentum map (right) of the 1:1:2 resonant oscillator system with Hamiltonian $H_{n,l}=S$.

The doubly reduced system has one degree of freedom. Trajectories of this system can be found as intersections $\{H_{n,l}=h\} \cap P_{n,l}$ of the constant h -level sets of the reduced Hamiltonian $H_{n,l}$ and the phase space $P_{n,l}$. It is simpler to work on the space $V_{n,l}=P_{n,l}/(\mathbb{Z}_2 \times \mathbb{Z}_2)$ obtained by reducing the discrete symmetries. This space is defined by

$$\tau + S^2 = (R - l^2)(n - R), \text{ where } n \geq R \geq |l| \geq 0 \text{ and } \tau = T^2 \geq 0$$

with boundary $\partial V_{n,l}$ given by

$$S^2 = (R^2 - l^2)(n - R), \quad n \geq R \geq |l| \geq 0$$

and study $\{H_{n,l}(R, S)=h\} \cap V_{n,l}$.

The lowest order approximation studied in Ref. 11 is sufficient for a qualitative description. As usual, we use the rescaled and shifted energy function $H_{n,l}(R, S)=S$.

Lemma A.1: The intersections $\{S=h\} \cap V_{n,l}$ are of three kinds:

- (i) one regular point of $\partial V_{n,l}$;
- (ii) a closed interval, whose endpoints are regular points of $\partial V_{n,l}$, that is, any point except point $(R, S)=0$ of $V_{n,0}$;
- (iii) a closed interval whose one endpoint is a regular point of $\partial V_{n,0}$ and the other is the singular point $(R, S)=0$.

Every sufficiently small generic deformation of the Hamiltonian function S has three types of level sets on $V_{n,l}$.

Proof: The level sets of the Hamiltonian function S are straight vertical lines in the plane with coordinates (R, S) . From (A9a) which defines $\partial V_{n,l}$ when $T=0$ we can see that these lines touch $\partial V_{n,l}$ at the points

$$R_c = \frac{1}{3}(n + \sqrt{n^2 + 3l^2}), \quad S_c = \pm \sqrt{(n - R_c)(R_c^2 - l^2)}, \tag{A12}$$

where S reaches its maximum and minimum value. □

3. Energy-momentum map

The image U of the energy-momentum map,

$$\mathcal{EM}: TR^3 \rightarrow U \subset R^3: (q, p) \rightarrow (L(q, p), H(q, p), N(q, p)),$$

is a three-dimensional domain in R^3 with coordinates (l, h, n) . In the first approximation with $H=S$, Eqs. (A12) and inequalities $n \geq 0, |l| \leq n$ define the boundary ∂U . It can be seen that $U \cap \{n=0\}$ is the point $(0,0,0)$, while for any $n > 0$ the constant n slice of U has the same topology of a closed disc with two singular points on the boundary and one isolated singular point inside, see Fig. 12 (left).

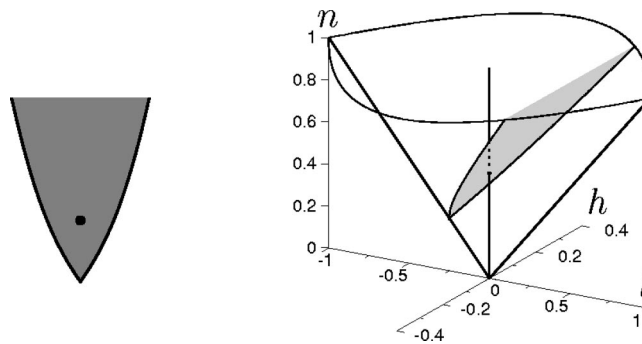


FIG. 13. Constant $n+l$ slice of the image of the energy-momentum map of the 1:1:2 resonant oscillator system with Hamiltonian $H_{n,l}=S$.

It can be seen that the whole domain U is a solid cone which has three curves of distinguished singular values: one is a thread inside U , the n axis, the other two are lines that lie on the boundary ∂U (the lines $l = \pm n, h = 0$), see Fig. 12 (right).

Note that different slices of U can be considered, see for example, the slice with constant $n + l$ in Fig. 13. All such slices have a topology of half-plane with one isolated singular point inside and one singular point on the boundary.

The fibers of the energy momentum map reconstruct as follows. The regular values shown as shaded area in Fig. 12 lift to regular 3-tori. The points in the smooth part of the boundary with $S \neq 0, N > 0$ lift to relative equilibria \mathbb{T}^2 , while singular points of the boundary with $S = 0, N > 0$ lift to relative equilibria S^1 . The points in the singular thread with $N > 0$ and $S = L = 0$ correspond to a special singular 3D fiber \mathfrak{F}_n whose topology can be best represented using two partial reduction maps, one with respect to the $SO(2)$ symmetry, the other with respect to the oscillator symmetry S^1 . As illustrated in Fig. 14 the former gives a curled torus while the latter gives a pinched torus.

APPENDIX B: DETAILS OF THE QUANTUM DESCRIPTION

Our quantum-mechanical investigation deals with the quantum system associated to the classical system whose Hamiltonian is the swing spring Hamiltonian normalized to third or sixth order. We use the quantum expression of the Hamiltonian expanded up to sixth order when discussing the range of energy levels at which our analysis is reasonable for applications, and its truncation at third order for the description of the 3D quantum lattice. In this section we explicitly write the expression of the operators associated to the four invariants appearing in the expansion of the Hamiltonian in a basis in which the operators \hat{N} and \hat{L} are diagonal.

In quantum mechanics one associates to a classical (polynomial) Hamiltonian H its quantized operator \hat{H} . The rule to obtain \hat{H} follows straightforwardly from the following ansatz (here stated for 1D systems): the domain of the operator is the Hilbert space with basis $|n\rangle$ ($n \in \mathbb{N}$); the

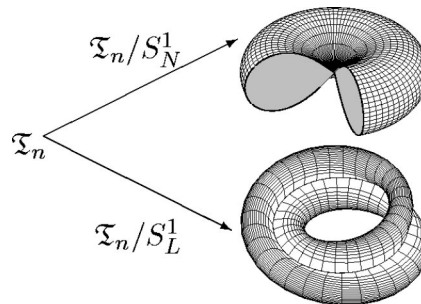


FIG. 14. Partial reduction of the singular 3D fiber.

operators $a=(1/\sqrt{2})(\hat{q}+i\hat{p})$ and $a^\dagger=(1/\sqrt{2})(\hat{q}-i\hat{p})$ act on the basis vectors as follows: $a|n\rangle=\sqrt{n}|n-1\rangle$ and $a^\dagger|n\rangle=\sqrt{n+1}|n+1\rangle$. In this treatment, we express every polynomial in p, q using the variables $(1/\sqrt{2})(q+ip)$ and $(1/\sqrt{2})(q-ip)$ and hence we define its associated quantum operator by replacing such variables with the operators a and a^\dagger , being careful to symmetrize the expressions (the variables of a polynomial commute, a and a^\dagger do not).

In our 3D case, the basis elements of the Hilbert space are denoted by $|n_1, n_2, n_3\rangle$, while the basic operators are called $a_1, a_1^\dagger, a_2, a_2^\dagger, a_3, a_3^\dagger$. With these notations, the classical polynomial $\frac{1}{2}(q_1^2+p_1^2)$ becomes the quantum operator $\frac{1}{2}(a_1a_1^\dagger+a_1^\dagger a_1)$. This operator associates to the basis vector $|n_1, n_2, n_3\rangle$ the vector $(n_1+1/2)|n_1, n_2, n_3\rangle$.

It follows that the quantizations of the functions playing a role in the completely integrable system $(H_{\text{nf}}^{(6)}, L, N)$ are

$$\hat{N} = \frac{1}{2}(a_1a_1^\dagger + a_1^\dagger a_1 + a_2a_2^\dagger + a_2^\dagger a_2 + 2a_3a_3^\dagger + 2a_3^\dagger a_3), \quad \hat{S} = \sqrt{2}i(a_1^\dagger a_2^\dagger a_3 - a_1 a_2 a_3^\dagger),$$

$$\hat{R} = \frac{1}{2}(a_1a_1^\dagger + a_1^\dagger a_1 + a_2a_2^\dagger + a_2^\dagger a_2), \quad \hat{L} = \frac{1}{2}(-a_1a_1^\dagger - a_1^\dagger a_1 + a_2a_2^\dagger + a_2^\dagger a_2).$$

The action of these operators on the generic vector $v=|n_1, n_2, n_3\rangle$ is

$$\hat{N}v = (n_1 + n_2 + 2n_3 + 2)v, \quad \hat{L}v = (n_1 - n_2)v, \quad \hat{R}v = (n_1 + n_2 + 1)v,$$

$$\hat{S}v = i\sqrt{2(n_1+1)(n_2+1)n_3}v^+ - i\sqrt{2n_1n_2(n_3+1)}v^-,$$

where $v^- = |n_1-1, n_2-1, n_3+1\rangle$ and $v^+ = |n_1+1, n_2+1, n_3-1\rangle$.

To plot the two-dimensional quantum diagrams in Fig. 3, we fix an eigenspace for the operator \hat{N} , that is, we fix a *polyad number*, and then compute the joint spectrum of the operators \hat{L} and $\hat{H}_{\text{nf}}^{(6)}$ in that eigenspace. The eigenspace associated to the eigenvalue $m+2$ is generated by all the vectors $|n_1, n_2, n_3\rangle$ such that $n_1+n_2+2n_3=m$. Observe that there are essentially two cases, depending on the parity of m . If m is even, the \hat{N} -eigenspace associated to the eigenvalue $m+2$ decomposes in the direct sum of eigenspaces for \hat{L} , $V_h = \mathbb{R}\{v_{h,k} = |k, h+k, \frac{1}{2}(m-h-2k)\rangle | k=0, \dots, \frac{1}{2}(m-h)\}$, where h , the \hat{L} -eigenvalue associated to V_h , runs over all even numbers from $-m$ to m . Here $\mathbb{R}\{v_{h,k}\}$ stands for real span of the vectors $v_{h,k}$. The dimension of V_h is $\frac{1}{2}(m-h)+1$. On each subspace V_h the operator \hat{L} is the scalar multiplication by h while \hat{S} acts as the tridiagonal matrix

$$\hat{S}v_{h,k} = i\sqrt{(k+1)(h+k+1)(m-h-2k)}v_{h,k+1} - i\sqrt{k(h+k)(m-h-2k+2)}v_{h,k-1}. \quad (\text{B1})$$

If m is odd, the \hat{N} eigenspace associated to the eigenvalue $m+2$ decomposes into \hat{L} eigenspaces $V_h = \mathbb{R}\{|k, h+k, \frac{1}{2}(m-h-2k)\rangle | k=0, \dots, \frac{1}{2}(m-h)\}$ indexed by all odd numbers from $-m$ to m . The dimension of V_h is $\frac{1}{2}(m-h)+1$. The operator \hat{H} acts on V_h according to (B1). These operators have been used to plot the quantum diagram of the swing spring.

To quantize the Hamiltonian $H_{\text{nf}}^{(6)}$ (4) and model the swing spring system for higher energy levels one can push further the process described above. Since the operators \hat{N} and \hat{L} commute with all the other operators, there is no difficulty in defining the operators $\widehat{NR}, \widehat{L}^2, \widehat{R}^2, \widehat{NR}^2, \widehat{NS}$, and \widehat{S}^2 . The only two noncommuting operators are \hat{R} and \hat{S} , for this reason \widehat{RS} acts on the vectors as $\frac{1}{2}(\hat{R}\hat{S} + \hat{S}\hat{R})$. The matrix of the quantum analog of the Hamiltonian $\hat{H}_{\text{nf}}^{(6)}$ on the vector space V_h with respect to the basis $v_{h,k}$ is pentadiagonal and depend on the physical variable \hbar , but we will not write here its expressions.

Another quantum diagram, displayed in Fig. 4, can be obtained by slicing the 3D quantum diagram by means of different momenta coming from the T^2 symmetry. To work with momenta that define an effective torus action, the authors of Ref. 11 use the functions $N_1 = \frac{1}{2}(N-L), N_2 = \frac{1}{2}(N+L)$. In q_i, p_i variables

$$N_1 = \frac{1}{2}(q_1^2 + p_1^2 + q_3^2 + p_3^2), \quad N_2 = \frac{1}{2}(q_2^2 + p_2^2 + q_3^2 + p_3^2), \quad H_{\text{nf}}^{(3)} = \hbar(N_1 + N_2) - \frac{3}{16}\hbar^{3/2}S.$$

The quantization of the functions N_1 and N_2 is

$$\hat{N}_1 = \frac{1}{2}(a_1 a_1^\dagger + a_1^\dagger a_1 + a_3 a_3^\dagger + a_3^\dagger a_3), \quad \hat{N}_2 = \frac{1}{2}(a_2 a_2^\dagger + a_2^\dagger a_2 + a_3 a_3^\dagger + a_3^\dagger a_3).$$

Again, one can restrict the analysis to the eigenspaces of the operator \hat{N}_1 corresponding to the eigenvalue $m+1$. In this case, the eigenspace of \hat{N}_1 is not finite dimensional, but it still can be decomposed into direct sum of subspaces,

$$W_h = \begin{cases} \mathbb{R}\{|m, h, 0\rangle, |m-1, h-1, 1\rangle, \dots, |m-h, 0, h\rangle\}, & \text{when } h < m, \\ \mathbb{R}\{|m, h, 0\rangle, |m-1, h-1, 1\rangle, \dots, |0, h-m, m\rangle\}, & \text{when } h \geq m. \end{cases}$$

Note that $\dim W_h = \begin{cases} h+1, & \text{when } h < m \\ m+1, & \text{when } h \geq m \end{cases}$. On each space W_h , the operator \hat{N}_2 acts as the multiplication by $h+1$; whereas the operator $\hat{H}_{\text{nf}}^{(3)}$ acts as the tridiagonal matrix

$$\begin{aligned} \hat{H}_{\text{nf}}^{(3)} v_{h,k} = & \frac{3}{16}\hbar^{3/2}i\sqrt{2(m-k)(h-k)(k+1)}v_{h,k+1} + \hbar(m+h+2)v_{h,k} \\ & - \frac{3}{16}\hbar^{3/2}i\sqrt{2(m-k+1)(h-k+1)}kv_{h,k-1}. \end{aligned} \tag{B2}$$

Here $v_{h,k}$ is the vector $|m-k, h-k, k\rangle$. These operators are the ones used to numerically plot Fig. 4 (right). The technique to obtain the slices with fixed quantum numbers n_{K_m} is very similar to the ones described above.

¹Colin de Verdière, Y. and Vũ Ngọc, S., “Singular Bohr–Sommerfeld rules for 2D integrable systems,” *Ann. Sci. Ec. Normale Super.* **36**, 1–55 (2003).
²Cushman, R.H., “Geometry of the energy-momentum mapping of the spherical pendulum,” *Centrum voor Wiskunde en Informatica Newsletter* **1**, 4–18 (1983).
³Cushman, R.H. and Bates, L., *Global Aspects of Classical Integrable Systems* (Birkhäuser, Basel, 1997).
⁴Cushman, R.H., Dullin, H.R., Giacobbe, A., Holm, D.D., Joyeux, M., Lynch, P., Sadovskii, D.A., and Zhilinskiĭ, B.I., “The CO₂ molecule as a quantum realization of the 1:1:2 resonant swing-spring system with monodromy,” *Phys. Rev. Lett.* **93**, 024302 (2004).
⁵Cushman, R.H. and Duistermaat, J.J., “The quantum mechanical spherical pendulum,” *Bull. Am. Math. Soc.* **19**, 475–479 (1988).
⁶Cushman, R.H. and Duistermaat, J.J., “Non-Hamiltonian monodromy,” *J. Diff. Eqns.* **172**, 42–58 (2001).
⁷Cushman, R.H. and Vũ Ngọc, S., “Sign of the monodromy for Liouville integrable systems,” *Ann. Inst. Henri Poincaré, Anal. Non Linéaire* **3**, 883–894 (2002).
⁸Cushman, R.H. and Zhilinskiĭ, B.I., “Monodromy of a two degree of freedom Liouville integrable system with many focus-focus points,” *J. Phys. A* **35**, L415–L419 (2002).
⁹Duistermaat, J.J., “On global action-angle coordinates,” *Commun. Pure Appl. Math.* **23**, 687–706 (1980).
¹⁰Duistermaat, J.J. and Heckman, G.J., “On the variation in the cohomology of the symplectic form of the reduced phase space,” *Invent. Math.* **69**, 259–269 (1982).
¹¹Dullin, H., Giacobbe, A., and Cushman, R.H., “Monodromy in the resonant swing spring,” *Physica D* **190**, 15–37 (2004).
¹²Efstathiou, K., Joyeux, M., and Sadovski, D., “Global bending quantum number and the absence of monodromy in the HCN ↔ CNH molecule,” *Phys. Rev. A* **69**, 032504 (2004).
¹³Fermi, E., “Über den Ramaneffekt des Kohlendioxyds,” *Z. Phys.* **71**, 250–259 (1931).
¹⁴Grondin, L., Sadovskii, D.A., and Zhilinskiĭ, B.I., “Monodromy as topological obstruction to global action-angle variables in systems with coupled angular momenta and rearrangement of bands in quantum spectra,” *Phys. Rev. A* **65**, 012105 (2002).
¹⁵Guillemin, V., *Moment Maps and Combinatorial Invariants of Hamiltonian Tⁿ-Spaces* (Birkhäuser, Boston, 1994).
¹⁶Hitzl, D.L. “The swinging spring-invariant curves formed by periodic solutions. III,” *Astron. Astrophys.* **41**, 187–198 (1975).
¹⁷Holm, D.D. and Lynch, P., “Stepwise precession of the resonant swinging spring,” *SIAM J. Appl. Dyn. Syst.* **1**, 44–64 (2002).
¹⁸Jacobson, M.P. and Child, M.S., “Spectroscopic signature of bond breaking internal rotation. II. Quantum monodromy and Coriolis coupling in HCP,” *J. Chem. Phys.* **114**, 262–275 (2001).
¹⁹Lewerenz, M. and Quack, M., “Vibrational spectrum and potential energy surface of the CH chromophore in CHD₃,” *J. Chem. Phys.* **88**, 5408–5432 (1988).
²⁰Michel, L. and Zhilinskiĭ, B.I., “Symmetry, invariants, topology: Basic tools,” *Phys. Rep.* **341**, 11–84 (2001).
²¹Nekhoroshev, N.N., “Action angle variables and their generalization,” *Trans. Mosc. Math. Soc.* **26**, 180–198 (1972).

- ²²Nekhoroshev, N.N., Sadovskii, D.A., and Zhilinskiĭ, B.I., "Fractional monodromy of nonlinear resonant oscillator," C. R. Acad. Sci., Ser. I: Math. **335**, 985–988 (2002).
- ²³Vũ Ngọc, S., "Quantum monodromy in integrable systems," Commun. Math. Phys. **203**, 465–479 (1999).
- ²⁴Sadovskii, D.A. and Zhilinskiĭ, B.I., "Counting levels within vibrational polyads. Generating function approach," J. Chem. Phys. **103**, 10520–10536 (1995).
- ²⁵Sadovskii, D.A. and Zhilinskiĭ, B.I., "Monodromy, diabolic points, and angular momentum coupling," Phys. Lett. A **256**, 235–244 (1999).
- ²⁶Zhilinskiĭ, B.I., "Hamiltonian monodromy as lattice defect," quant-ph/0303181.
- ²⁷Zung, N.T., "Another note on focus-focus singularities," Lett. Math. Phys. **60**, 87–99 (2002).